3D scanning by means of dual-projector structured light illumination

Daniel L. Lau[a] and Ying Yu[a]

[a]University of Kentucky, Address, Lexington, US;

ABSTRACT

This document shows the desired format and appearance of a manuscript prepared for the Proceedings of the SPIE. It contains general formatting instructions and hints about how to use LaTeX. The LaTeX source file that produced this document, `article.tex` (Version 3.3), provides a template, used in conjunction with `spie.cls` (Version 3.3).

Keywords: Manuscript format, template, SPIE Proceedings, LaTeX

1. INTRODUCTION

As one of the non-contact 3D shape measurement techniques, the structured light illumination (SLI) has been known for its high resolution and high speed.[1] Conventional SLI systems consist of one projector, one camera and one processing unit which is usually a computer. The projector presents patterns that are encoded with some information related to the pixel locations on the object to be measured. If the projection is on a flat surface, the patterns seen should be identical to its original design. However, with the presence of the non-planar object under the projection, what is actually seen from the camera is the distorted patterns on the surface of the object. By comparing and analyzing the distortion in the images taken by the camera, the 3D surface of the object can eventually be reconstructed in a processing unit.

Within the scope of this fundamental idea and system structure, a lot of research has been done over the past several decades.[2] Different practical implementations have been proposed, from pattern design to system calibration, then to the algorithms that are used to decode the captured patterns. One widely studied area is the one-shot SLI strategy in which only one static pattern is projected onto the object. It employs color pattern,[3] binary grid pattern,[4] gray-scale pattern[5] or even composite pattern.[6] Since there is only one image need to be processed for a scan, the 3D reconstruction can be completed fast. The one-shot strategy is ideal for high speed applications such as real time scanning. But in terms of accuracy, it is not so promising compared to some multi-shot SLI strategy in which the 3D reconstruction is derived by projecting a sequence of patterns and processing multiple images.[7]

According to the method of encoding the information containing the pixel location into the pattern, phase measuring profilometry (PMP)[8] is a subset of SLI techniques that acquires the depth value by translating the phase data from the projected patterns pixelwise. The PMP has some advantageous features including its insensitivity to ambient light and its high accuracy.[9,10] Higher frequency patterns have been introduced to PMP systems to reduce the effects of the noise and achieve higher accuracy.[11] Nonetheless, higher frequency patterns also produces the phase ambiguity which requires the system to execute some extra computation called phase unwrapping.[12] Furthermore, adding high frequency patterns increases the projection time as well as the number of images to be processed, which accordingly decreases the overall speed of the system. Liu *et al.* proposed an ingenious dual-frequency pattern strategy which combines a high-frequency pattern and a unit-frequency pattern into one composite pattern,[13] it improved the accuracy without increasing the scanning time.

In this paper, we propose a dual-projector, dual-frequency SLI scheme and its practical implementation. Unlike the scanner presented by XXXX,[?] the proposed scanner projects patterns from both projectors simultaneously, which keeps the scan time the same versus a single projector scanner. We also allow the projectors to

Further author information: (Send correspondence to A.A.A.)
A.A.A.: E-mail: aaa@tbk2.edu, Telephone: 1 505 123 1234
B.B.A.: E-mail: bba@cmp.com, Telephone: +33 (0)1 98 76 54 32

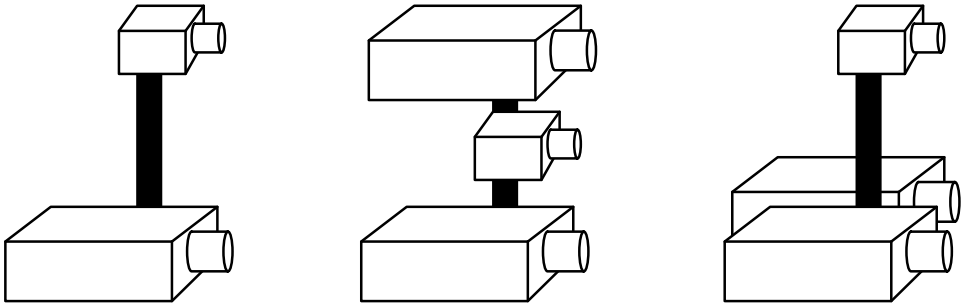

Figure 1: Structured light scanners composed of (left) a single projector, (center) opposed dual-projectors for wrap around scanning, and (right) complementary dual-projectors for increased luminance.

be placed in any arbitrary arrangement with 3D point clouds generated from a single fused phase image instead of fusing to independently generated point clouds. Depending on the arrangements of projectors as illustrated in Fig. 1, a dual-projector SLI scanner can be used to minimize occlusions[14] since a scan surface needs to be visible to at least one projector and the camera. So placing projectors in opposition means a face, for example, can be illuminated from both sides. Having two unique paths of light from projector to camera also creates new opportunities and challenges for overcoming the issue of muti-path.[15]

Placing projectors side-by-side can be used to achieve twice the luminance of a single projector. For instance, suppose the projectors we use are two identical Optoma ML750ST which has around 500 lumens each,[16] by using two projectors, we obtain a total 1000 lumens. Higher light intensity gives rise to the higher signal-to-noise ratios (SNR),[17] which makes the system less susceptible to sensor noise, consequently the system becomes more robust and accurate.

Now in order for dual-projector SLI scanners to become practical, there are two fundamental problems that need to be addressed. The first is the practical implementation of control logic to perfectly synchronize the projectors to a camera. For this, we describe an FPGA-based controller using a commodity FPGA board to simultaneously drive two HDMI ports. The advantage of this system is that it allows us to avoid the practical issues associated with modern GPUs as well as staying low cost. The second problem that needs to be addressed is how to perform phase unwrapping when the phase images derive from separate projectors arbitrarily arranged. Using the dual-frequency pattern scheme, we demonstrate using a unit-frequency phase image from one projector to unwrap the high-frequency phase image in the second, opposed projector, using a look-up table-based operation ideally suited for GPUs. This real-time approach is highly flexible and can be used to replace phase unwrapping schemes such as the Chinese remainder technique of XXXX.[?]

2. DUAL-FREQUENCY PHASE MEASURING PROFILOMETRY

The dual-frequency pattern scheme was initially proposed by Liu *et al.*,[13] it is essentially an improved derivation of the phase measuring profilometry.[10] In the the traditional PMP a series of phase-shifting sinusoidal fringe patterns are projected onto the object to be measured, the fringe patterns can be either horizontal or vertical, the presence of the object distorts the patterns, then by analyzing the phase values in the deformed pattern images, the 3D depth values can be obtained.

Suppose the phase-shifting patterns are vertical, which indicates that all the pixels in a same row have the identical intensity, and from top to bottom the value of intensities in each row form a sinusoidal function. Therefore, this kind of PMP patterns can be generalized as:

$$I_n^p(x^p, y^p) = A^p + B^p \cos(2\pi f y^p - \frac{2\pi n}{N}), \tag{1}$$

where I_n^p is the intensity of the pixel at the coordinate (x^p, y^p) from the projector's point of view; A^p is background intensity which is considered as a constant; B^p is another constant which represents the fringe contrast compared to the background; f is the frequency of the fringe pattern set which is equal to the number of sinusoidal periods

from top to the bottom of the projected patterns; N is the total number of the phase-shifting patterns of the same frequency in a set, n is the current number of the pattern within the range of $[0, N-1]$.

On the camera's side, the image of the object under the projection of each unique PMP pattern is captured as part of the data to reconstruct the 3D profile of the object. So the projected scene of the object can be described as eq. (2) from the camera's point of view,

$$I_n^c(x^c, y^c) = A^c(x^c, y^c) + B^c(x^c, y^c)\cos(\phi(x^c, y^c) - \frac{2\pi n}{N}), \tag{2}$$

where I_n^c is the intensity of the given pixel (x^c, y^c) in the camera's coordinates system; $A^c(x^c, y^c)$ is the average intensity of the given pixel over the N patterns; B^c can be considered as the average intensity of the PMP pattern seen by the camera, so for any given pixel (x^c, y^c) in a pattern set $[0, N-1]$, A^c and B^c are both constant, furthermore, $B^c(x^c, y^c)$ can be derived from eq. (2) as:

$$B^c(x^c, y^c) = \frac{2}{N}\sqrt{\left[\sum_{n=0}^{N-1} I_n^c(x^c, y^c)\sin(\frac{2\pi n}{N})\right]^2 + \left[\sum_{n=0}^{N-1} I_n^c(x^c, y^c)\cos(\frac{2\pi n}{N})\right]^2}. \tag{3}$$

In Equation 2, there is another important constant ϕ for any given pixel (x^c, y^c) in a given pattern set $[0, N-1]$, it is the phase value $\phi(x^c, y^c)$ of the distorted fringe patterns that is eventually used to calculate the corresponding depth value of the object. The expression of $\phi(x^c, y^c)$ can be inferred from eq. (3) as:

$$\phi(x^c, y^c) = \arctan\frac{\sum_{n=0}^{N-1} I_n^c(x^c, y^c)\sin(\frac{2\pi n}{N})}{\sum_{n=0}^{N-1} I_n^c(x^c, y^c)\cos(\frac{2\pi n}{N})}. \tag{4}$$

The dual-frequency pattern scheme adds a second sinusoidal component to the phase-shifting patterns, as a result, the total number of patterns is still N, but each pattern has two sinusoidal components, one is of unit frequency f_u, the other is of a high frequency f_h that is used to reduce the impact of noises in the system. If we extend the single-frequency PMP pattern above to the dual-frequency, the intensities of the row pixels from top to bottom would be like an amplitude modulation in which the f_u is frequency of the modulating signal and f_h is the frequency of the carrier wave. According to Liu *et al.*, from the projector's point of view, the new dual-frequency pattern is expressed as:

$$I_n^p(x^p, y^p) = A^p + B_1^p\cos(2\pi f_h y^p - \frac{2\pi n}{N}) + B_2^p\cos(2\pi f_u y^p - \frac{4\pi n}{N}), \tag{5}$$

where the I_n^p is the intensity of the pixel (x^p, y^p) in the n^th pattern. Similarly the intensity equation of the camera coordinates used for reconstruction becomes:

$$I_n^c(x^c, y^c) = A^c(x^c, y^c) + B_1^c(x^c, y^c)\cos(\phi_h(x^c, y^c) - \frac{2\pi n}{N}) + B_2^c(x^c, y^c)\cos(\phi_u(x^c, y^c) - \frac{4\pi n}{N}). \tag{6}$$

Likewise the B_1^c, B_2^c and ϕ_h, ϕ_u can be derived from eq. (3) and eq. (4) respectively,

$$B_m^c(x^c, y^c) = \frac{2}{N}\sqrt{\left[\sum_{n=0}^{N-1} I_n^c(x^c, y^c)\sin(m\frac{2\pi n}{N})\right]^2 + \left[\sum_{n=0}^{N-1} I_n^c(x^c, y^c)\cos(m\frac{2\pi n}{N})\right]^2}, \tag{7}$$

where $m = 1$ *or* 2 in this case,

$$\phi_h(x^c, y^c) = \arctan\frac{\sum_{n=0}^{N-1} I_n^c(x^c, y^c)\sin(\frac{2\pi n}{N})}{\sum_{n=0}^{N-1} I_n^c(x^c, y^c)\cos(\frac{2\pi n}{N})}, \tag{8}$$

$$\phi_u(x^c, y^c) = \arctan\frac{\sum_{n=0}^{N-1} I_n^c(x^c, y^c)\sin(\frac{4\pi n}{N})}{\sum_{n=0}^{N-1} I_n^c(x^c, y^c)\cos(\frac{4\pi n}{N})}. \tag{9}$$

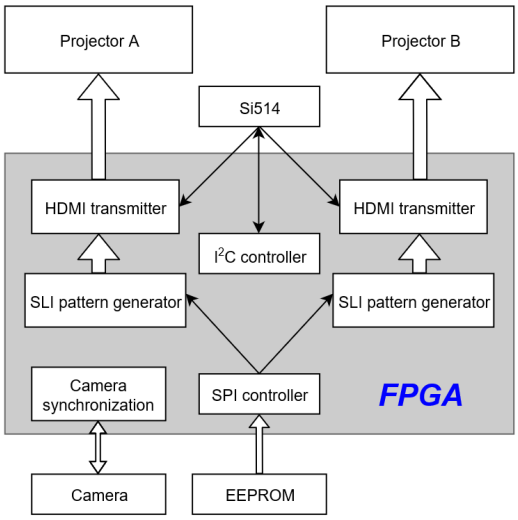

Figure 2: System diagram

Now in eqns. (8) and (9), ϕ_h and ϕ_u are confined within $[-\pi, \pi]$; however, the actual range of ϕ_h is $[0, 2f_h\pi]$, the ϕ_h is called the wrapped phase. Unwrapping the ϕ_h to $\tilde{\phi_h} \in [0, 2f_h\pi]$ can lead to a more accurate conversion from phase to depth. In order to obtain $\tilde{\phi_h}$, the value of ϕ_u is used as the following equation shows,

$$\tilde{\phi_h} = \phi_h + 2\pi\lfloor\frac{\phi_u}{2\pi/f_h}\rfloor, \tag{10}$$

where the $\lfloor\rfloor$ is the symbol of floor function which outputs the greatest integer less than or equal to the value enclosed.

3. DUAL-PROJECTOR PHASE MEASURING PROFILOMETRY

Our FPGA-based dual-projector Structured Light Illumination (SLI) system generates two synchronized SLI patterns which are then fed to two projectors via HDMI. Meanwhile, the projectors and the camera need to be synchronized to ensure that the camera images are taken at the right timing. The system diagram is shown in Figure 2. The two SLI pattern generators output two synchronized phase-shifting fringe patterns which are later encoded into TMDS data streams by the HDMI transmitters and eventually move to projectors.

HDMI is the abbreviation of High-Definition Multimedia Interface, it is one of the most popular display interfaces. The newest release, HDMI Version 2.1 supports up to $10K$ video at $120Hz$. A standard HDMI connector has 19 pins as listed in Table 1. Data channel 2, 1, 0 are mainly used to transfer red, green and blue components of the video respectively. The HDMI does not only transfer video data, but also some auxiliary data, for example audio data, packet header. The auxiliary data, video data as well as some control signals are encoded in data channel 2, 1, 0 and then digitally transmitted in serial. In between any two adjacent video periods, one or more data island period and control period are inserted.

In HDMI, there are six important control signals, HSYNC indicates the beginning and end of a row in a frame of the video, VSYNC indicates the beginning and end of a frame, CTL0 CTL3 indicate the data type of the following data period. The three data channels are transmitted through a differential signaling technology called Transition-Minimized Differential Signaling (TMDS) to reduce the impact of electromagnetic interference and enable high clock skew tolerance.

The 5 volts power signal is provided by the HDMI source or an external source, which after the HDMI sink reads the 5 volts signal, it immediately asserts the pin, Hot Plug Detect. Once the HDMI source detects the presence of a sink by the assertion of the pin Hot Plug Detect, it sends an I^2C-based command of a read request

to the sink. The pins SCL and SDA compose the display data channel (DDC) via which the Extended Display Identification Data (EDID) is read by the HDMI source from the sink as the response to the read request. The EDID is usually 128 or 256 bytes long, it contains various information related to the features of display system, including but not limited to, manufacturer ID, serial number, week and year of manufacture, screen size, supported timing, etc.

The pin CEC is used to add some advanced functionalities for the HDMI systems. Usually it is a remote control that issues different high-level commands to the devices connected by HDMI cables. CEC stands for Consumer Electronics Control, it is also a one-wire bus protocol, the implementation of CEC is optional, because not all the HDMI devices support this feature. Since HDMI 1.4, the previously reserved pin has become the HDMI Ethernet and Audio Returen Channel (HEAC). While it is in audio return channel mode, only the HEAC+ line is used to transmit audio data; in HDMI Ethernet channel mode, the HEAC+ line pairs up with the HEAC- line as a differential signal to establish a high speed Ethernet communication.

To obtain the uncommon 73.25 MHz pixel clock for 800×600 pixel video at 120 Hz which cannot be generated by the Spartan 6 of the Mojo board, we utilize a programmable oscillator, the Si514. By configuring the internal registers through I^2C bus, Si514 can generate any frequency from 100 kHz to 250 MHz with a tuning resolution of 0.026 ppb. Therefore, an I^2C master controller was incorporated into the system...what parameters did you use to get the clock rate with this oscillator.

Now in order to linearize the projector to avoid the deleterious effects of gamma distortion[18] on our projected PMP patterns, we use the EEPROM of the Mojo board to upload calibrated tone correction curves for our target projector...JUST SAY SOMETHING ABOUT HOW THE LUT IS PROGRAMMED OVER SERIAL COMMUNICATION WITH MICROCONTOLLER AND THAT IT IS READ DURING BOOT UP OF THE FPGA TO THE INTERNAL LUT INSIDE YOUR BIT FILE...This LUT can be hard-coded into the configuration file of the FPGA, but the drawback is that once the lookup table changes, the FPGA configuration file has to be changed. It is quite inconvenient especially when the system needs to be often applied to a different projector, because generating a new FPGA configuration file requires special software tool and takes more time. We devise a method that the user stores the LUT in an separate EEPROM chip which can be erased and written by any computer via some general serial or USB tools, and the SPI master module in the FPGA reads the EEPROM every time the system is powered on. With this approach, users can load new LUTs much faster and easier.

The camera synchronization module controls the timing of the camera trigger signal...DESCRIBE THE GPIO CONNECTIONS BETWEEN CAMERA AND PROJECTOR. IN PARTICULAR, YOU RECEIVE AN ENABLE BIT WHICH IS A PROGRAMMABLE GENERAL PURPOSE BIT FROM THE CAMERA TO THE FPGA THAT THE PC CAN ENABLE WHEN THE HOST PC IS READY TO PERFORM A SCAN. YOU THEN START PROJECTING THE FIRST PATTERN IN THE SEQUENCE AND WAIT FOR A SECOND BIT, THE FRAME TRIGGER READY BIT FROM THE CAMERA TO THE FPGA, THAT TELLS THE FPGA THAT IT IS READY FOR A TRIGGER. ON THE SUBSEQUENT VERTICAL SYNC, THE FPGA SENDS OUT A TRIGGER SIGNAL TO THE CAMERA. THE FPGA THEN STARTS PROJECTING THE NEXT PATTERN IN THE SEQUENCE WHILE WAITING FOR THE FRAME TRIGGER READY TO GO HIGH AGAIN. WHEN IT DOES, THE FPGA WAITS FOR THE NEXT VERTICAL SYNC TO SEND OUT

Table 1: HDMI pinout

PIN	DATA
Data2+, Data2 Shield, Data2-	red pixel component, CTL2, CTL3 and auxiliary data
Data1+, Data1 Shield, Data1-	green pixel component, CTL0, CTL1 and auxiliary data
Data0+, Data0 Shield, Data0-	blue pixel component, HSYNC, VSYNC and auxiliary data
Clock+, Clock Shield, Clock-	pixel clock
SCL, SDA	DDC channel, the source reads the EDID from the sink
CEC	data or commands from remote control
Reserved/HEAC+	reserved for v1.3 and before, Ethernet and audio since v1.4
HOT PLUG DETECT/HEAC-	indicate the hot plug or paired with HEAC+
+5V, Ground	power from external or HDMI source, ground

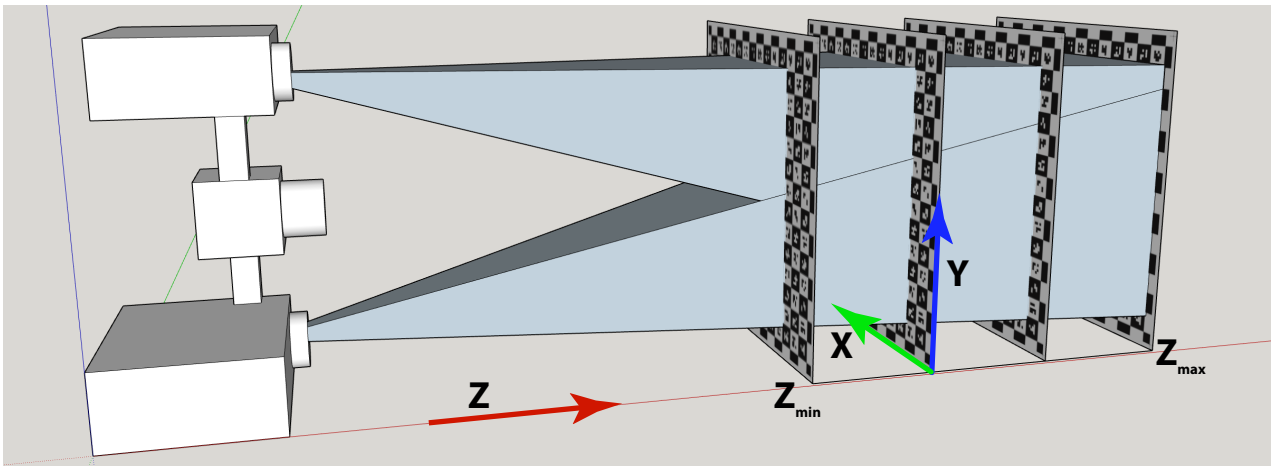

Figure 3: Illustration showing dual-projector scanner calibration.

A TRIGGER, MOVING TO THE NEXT PATTERN IN THE SEQUENCE. IT IS UP TO THE PC TO SET THE TRIGGER DELAY AND EXPOSURE TIME IN ORDER TO CAPTURE THE ONE FRAME OF VIDEO THAT CORRESPONDS TO THE PROJECTED PATTERNS. HOWEVER, THE TRIGGER READY SIGNAL CONTROLS THE FRAME RATE OF THE PROJECTOR TO INTEGER DIVISIONS OF 120 HZ, SUCH AS 120, 60, 40, 24, ETC DEPENDING ON THE BUS SPEED OF THE CAMERA. SO A GIGE CAMERA WITH A MAXIMUM OF 25 FPS WILL RUN AT 24 FPS.

4. CALIBRATION

The procedure for calibrating our scanner is illustrated in Fig. 3 and involves sweeping a rigid, flat checkerboard pattern, in correspondence with the XY-plane, in fixed, small-steps through the scan volume from the nearest plane at $Z = Z_{min}$ to the farthest plane at $Z = Z_{max}$. The physical moving of the checkerboard pattern is performed using a motorized rail like the Velmex Bi-slide and VXM controller. These rails can be configured to move with a positional accuracy of 0.076 mm and repeatability of 0.005 mm. The specific checkerboard pattern that we use is the CalTag calibration target introduced by Atcheson et al[?] where, inside each square, is a unique 16-bit codeword identifying and absolute world coordinates, (X_w, Y_w), of each square's four corners. Having this code word also means that portions of the target can be obscured from the camera's field of view or simply land outside of it. So we can calibrate the lens as close to the edge of the field as view as we like.

As stated above, the calibration procedure involves iteratively moving the CalTag target along the Z-axis from Z_{min} to Z_{max} such that, at each step, we perform a structured light scan with each camera pixel defined according to:

$$I_c[r, c, k] = [X_w[r, c, k], Y_w[r, c, k], Z_w[k], P[r, c, k]] \tag{11}$$

where r and c are the pixel's row and column coordinate; k is the step index for the current scan; $X_w[r, c, k]$ and $Y_w[r, c, k]$ are the CalTag grid coordinate at the intersection of the CalTag target's surface and the camera pixel's line-of-sight; $Z_w[k]$ is the Z-position of the rail; and $P[r, c, k]$ is the phase value of the projected PMP sequence in the line-of-sight of the camera pixel. Once complete, we then have a 3D texture composed of a stack of 4-color digital images that are the height and width of our camera and K layers deep with $P[r, c, k]$ ranging from $P_{min}[r, c]$ to $P_{max}[r, c]$ as $Z_w[k]$ ranges from Z_{min} to Z_{max}.

In order to parameterize the relationships between channels, let's define $\vec{x}_{r,c}$, $\vec{y}_{r,c}$, and $\vec{z}_{r,c}$ as the K-dimensional vectors composed of $X_w[r, c, k]$, $Y_w[r, c, k]$, and $Z_w[k]$, and let's define $\vec{p}_{r,c}$ as the normalized phase vector derived from $P[r, c, k]$ according to:

$$\vec{p}_{r,c}[k] = \frac{P[r, c, k] - P_{min}[r, c]}{P_{max}[r, c] - P_{min}[r, c]}. \tag{12}$$

From these vectors, we can derive a plot of any pixel channel versus any other channel. For example, we can plot $\vec{x}_{r,c}$ versus $\vec{z}_{r,c}$ or, more importantly, $\vec{z}_{r,c}$ versus $\vec{p}_{r,c}$. Assuming the pin-hole lens model for both the camera and the projector, we know from Liu *et al* that the relationship between $\vec{x}_{r,c}$ and $\vec{z}_{r,c}$ as well as $\vec{y}_{r,c}$ and $\vec{z}_{r,c}$ are given by the straight line relationships:

$$\vec{x}_{r,c} = A_{r,c}\vec{z}_{r,c} + B_{r,c}, \text{ and} \tag{13}$$

$$\vec{y}_{r,c} = C_{r,c}\vec{z}_{r,c} + D_{r,c}, \tag{14}$$

where $A_{r,c}$, $B_{r,c}$, $C_{r,c}$, and $D_{r,c}$ are scalar constants representing the slope and intercepts found by best-fitting straight lines between recorded points; furthermore, the relationship between $\vec{z}_{r,c}$ versus $\vec{p}_{r,c}$ is given by the equation:

$$\tilde{z}[r,c] = \frac{E_{r,c}\vec{p}_{r,c} + F_{r,c}}{G_{r,c}\vec{p}_{r,c} + H_{r,c}}, \tag{15}$$

where $E_{r,c}$, $F_{r,c}$, $G_{r,c}$, and $H_{r,c}$ are scalar constants found either through singular value decomposition[?] or the pseudo-inverse.[?] In situations where the lens of either the projector or the camera are not accurately modeled by the pin-hole lens model, we can replace eqn. (15) with a more flexible fourth-order polynomial model defined as:

$$\tilde{z}[r,c] = E_{r,c}\vec{p}_{r,c}^{\,4} + F_{r,c}\vec{p}_{r,c}^{\,3} + G_{r,c}\vec{p}_{r,c}^{\,2} + H_{r,c}\vec{p}_{r,c} + I_{r,c}, \tag{16}$$

where $E_{r,c}$, $F_{r,c}$, $G_{r,c}$, $H_{r,c}$, and $I_{r,c}$ are found using a least-squares polynomial fitting algorithm. Equation (14) need not change since the line-of-sight of any camera pixel is a straight line regardless of any lens distortion.

Now as an alternative to parameterizing our calibration data by eqns. (14)-(16), a wholly different approach is to build a 3D look-up-table indexed by the normalized phase values acquired during a scan. This is achieved by generating a set of plots between the world coordinates in $\vec{x}_{r,c}$, $\vec{y}_{r,c}$, and $\vec{z}_{r,c}$ versus $\vec{p}_{r,c}$ and then resampling them along equal increments of the $\vec{p}_{r,c}$ axis, keeping in mind that $\vec{x}_{r,c}$, $\vec{y}_{r,c}$, $\vec{z}_{r,c}$, and $\vec{p}_{r,c}$ are currently recorded at equal increments along $\vec{z}_{r,c}$. Keeping in mind that this interpolation can be with greater or fewer samples, L, than the original collected data with K layers. Doing so, we define our look-up-table as a 3D texture according to:

$$LUT[r,c,l] = [X_w[r,c,l], Y_w[r,c,l], Z_w[r,c,l]] \tag{17}$$

where r and c are the pixel's row and column coordinate and l is the resampled step index replacing k. The benefits of using the look-up-table over the parameterized model is that it avoids the error associated with inappropriate parameterization of lens distortion as well as detrimental impact of phase distortions such as gamma[?] or dithering noise when using projector defocus to blur the pixels of a binary spatial light modulator.[?] The only condition is that the phase image must be monotonic. With regards to real-time performance, the 3D look-up-table is easily implemented on an OpenGL shader using the *texture* function.[?]

ACKNOWLEDGMENTS

This work has been supported by Intel Corporation and the National Science Foundation under contract No. 1539157 and the Visual and Experiential Computing initiative. Dr. Daniel L. Lau is a Professor at the University of Kentucky and a Founder of Seikowave Inc., a private company that designs and sells structured light scanners.

REFERENCES

1. Chen, F., Brown, G. M., and Song, M., "Overview of three-dimensional shape measurement using optical methods," *Opt. Eng.* **39**, 10–22 (2000).
2. Geng, J., "Structured-light 3d surface imaging: a tutorial," *IEEE Intelligent Transportation System Society* (31 March 2011).
3. Wust, C. and Capson, D. W., "Surface profile measurement using color fringe projection," *Machine Vision and Applications* **4**, 193–203 (1991).
4. Grin, P. M., Narasimhan, L. S., and Yee, S. R., "Generation of uniquely encoded light patterns for range data acquisition," *Pattern Recog.* **25**(6), 609–616 (1992).

5. Durdle, N. G., Thayyoor, J., and Raso, V. J., "An improved structured light technique for surface reconstruction of the human trunk,," *IEEE Canadian Conference of Electrical and Computer Engineering* **2**, 874–877 (1998).
6. Guan, C., Hassebrook, L. G., Lau, D. L., Yalla, V., and Casey, C., "Improved composite-pattern structured-light profilometry by means of postprocessing," *Opt. Eng.* **47**(9), 0972031–09720311 (2008).
7. Blais, F., "A review of 20 years of range sensor developement," *Proceedings of SPIE-IS&T Electronic Imaging* **5013**, 62–76 (2003).
8. Srinivasan, H.C., Liu, H. C., and Halioua, M., "Automated phase measuring profilometry: a phase mapping approachl," *Appl. Opt.* **24**, 185–188 (1985).
9. C., G., Hassebrook, G., L., and Lau, D. L., "Composite structured light pattern for three-dimensional video," *Opt. Express* **11**(5) (10 March 2003).
10. Halioua, M. and Liu, H., "Optical three-dimensional sensing by phase measuring profilometry," *Opt. Lasers Eng.* **11**, 185–215 (1989).
11. Li, J., Hassebrook, L. G., and Guan, C., "Optimized two-frequency phase measuring profilometry light sensor temporal noise sensitivity," *J. Opt. Soc. Am.* **20**, 106–115 (2003).
12. Song, J., Ho, Y. S., Lau, D. L., and Liu, K., "Universal phase unwarpping for phase measuring profilometry using geometry analysis," *Proc. SPIE* **10546**, 0B0–0B8 (2018).
13. Liu, K., Wang, Y., Lau, D., Hao, Q., and Hassebrook, L. G., "Dual-frequency pattern scheme for high-speed 3-d shape measurement," *Opt. Express* (1 March 2010).
14. Lin, J., Jiang, K., and Chang, M., "A novel solution for camera occlusion in stereo vision technique," *Adv. Mech. Eng.* **2013**, 1–8 (2013).
15. O'Toole, M., Mather, J., and Kutulakos, K. N., "3d shape and indirect appearance by structured light transport," *IEEE Trans. Pattern Anal. Mach. Intell.* **38**(7), 1298–1312 (2016).
16. "Road test: optoma ml750st." `https://www.projectorcentral.com/optoma-ml750st-projector-review-road-test.htm`.
17. Wang, Y., Liu, K., Lau, D. L., Hao, Q., and Hassebrook, L. G., "Maximum snr pattern strategy for phase shifting methods in structured light illumination," *J. Opt. Soc. Am.* **27**(9), 1962–1971 (2010).
18. Liu, K., Y.Wang, Lau, D. L., Hao, Q., and Hassebrook, L. G., "Gamma model and its analysis for phase measuring profilometry," *J. Opt. Soc. Am.* **27**(3), 553–562 (2010).